

Detecting gamma-ray bursts from M31 with the wide field X-ray cameras on board BeppoSAX

Mateusz Ruszkowski^{1,2,3} and Ralph A. M. J. Wijers¹

¹*Institute of Astronomy, Madingley Road, Cambridge, CB3 0HA*

²*Warsaw University Astronomical Observatory, Al. Ujazdowskie 4, 00-478 Warsaw, Poland*

³*Nicolaus Copernicus Astronomical Center, Polish Academy of Sciences, Bartycka 18, 00-716 Warsaw, Poland*

Email: ruszkows@sirius.astro.uw.edu.pl and ramjw@ast.cam.ac.uk

Submitted to MNRAS, 21 January 1997

ABSTRACT

Gamma-ray bursters emit a small fraction of their flux in X rays, and because X-ray detectors are often very sensitive they may probe the gamma-ray burst universe more deeply than the current best gamma-ray instruments. On the reasonable assumptions that spectra of bursts observed by BATSE may be used to predict the X-ray fluxes of gamma-ray bursts, and that any corona of bursts around M31 is similar to the one around the Milky Way, we predict the rate at which the wide field cameras on board BeppoSAX should detect bursts from the Milky Way and M31. These rates are such that a one-month observation of M31 would have to either detect bursts from M31 or exclude most galactic models of gamma-ray bursts. (It is shown how the remainder can be dealt with.) Therefore such an observation would settle the long-standing dispute over their location.

Key words: gamma-ray bursts – X rays – galaxies: M31

1 INTRODUCTION

The results of the BATSE mission (see Fishman and Meegan 1995), combined with earlier data sets for bright bursts such as the one collected by PVO (Fenimore et al. 1993) have shown that (1) gamma-ray burst positions are distributed uniformly and randomly on the sky (Briggs et al. 1996a,b) and (2) the cumulative number as a function of peak flux, $N(> P_\gamma)$, is consistent with a constant rate density of bursts within some volume around us, and a decreasing density outside that volume. This implies that we are at the centre of a gamma-ray burst universe of which we can see the edge and which looks the same in all directions. Most distance scales are therefore excluded. The first remaining one is the high-redshift universe, with the edge being caused either by cosmological volume effects near and beyond $z = 1$ or by evolution of the density at moderate redshift (or both). The second one is an extended corona of our Galaxy, much bigger than the dark-matter halo and invented for the purpose of housing gamma-ray bursts (GRB). We are not strictly in its centre, but the average GRB distance can be made large enough that the anisotropy due to our offset from the centre is below the limit set by the BATSE data on burst positions. At the same time it can still be small enough that we need not see M31 (Briggs et al. 1996b). The aim of this paper is to demonstrate the capability of the Wide Field Cameras (WFC) on board BeppoSAX (launched in April 1996) to

distinguish between these options by searching for the hypothetical corona of GRB around M31. We first discuss the Z-ray detectability of GRB (Sect. 2) and our implementation of corona models (Sect. 3). Our results are presented in Sect. 4 and compared to previous results in Sect. 5.

2 X-RAY DETECTION OF GRB

Ginga observations and some earlier detections indicate that gamma-ray bursts emit some X rays (for an overview of early X-ray detections, see Preece et al 1996). It is only a small fraction of the flux (2% or so median; Laros et al. 1984, Yoshida et al. 1989), but since X- and gamma-ray instruments are photon counting devices it is the higher count rate ratio of X rays to gamma rays that matters. In addition, X-ray detectors usually have lower backgrounds because of their imaging capability. In all, they can see some fainter bursts than BATSE, the currently most sensitive gamma-ray detector looking for GRB, at a price of having a much smaller field of view. This was recently used by Hamilton et al. (1996) to constrain galactic-coronal models of GRB using archival Einstein data. They used galaxies typically a few Mpc away, the compromise distance for Einstein's exquisite sensitivity but very small field of view. The lower sensitivity of the WFC mean we should observe more nearby galaxies to constrain galactic-coronal models with them; the large

field of view means that we can go as close as M31 without losing too many bursts because they lie outside the field of view.

2.1 The WFCs on board SAX

There are two WFCs on board SAX, looking at opposite directions on the sky and perpendicular to the on-axis instruments. They are coded-mask imaging instruments with an entry mask of 256×256 1 mm^2 pixels placed 700 mm away from the detector plane. This leads to a response that is approximately triangular in both x and y and falls to zero 20° away from the optical axis along the x and y directions. It is sensitive to the energy range 1.6–32 keV. The response function was kindly supplied to us by Dr. J. Heise of SRON Utrecht. The angular resolution is a few arcminutes for bright sources. The 130 cts/s background of the instrument is mainly due to the diffuse extragalactic emission integrated over the field of view. The instrumental backgrounds are small and stable due to the low equatorial orbit which avoids the radiation belts and the South Atlantic Anomaly.

2.2 The X-ray fluxes of GRB

Previous workers have used a mean flux ratio of typically 2% between the BATSE flux and the X-ray flux of a gamma-ray burst. Rather than rely on the few X-ray detected gamma-ray bursts, we note that the WFC and BATSE sensitivity ranges overlap in the 10–30 keV range, and that therefore extrapolating the BATSE spectra into the WFC band should give reasonably good estimates of the expected SAX WFC count rates. Band et al. (1993) published detailed spectral fits to a sample of bright GRB from the first-year BATSE catalogue. The model consists of two power laws connected by a smooth transition at a break energy. Almost all break energies are well within the BATSE range. The model fits are shown in Fig. 1, scaled to a photon number flux of $1 \text{ phot cm}^{-2} \text{ s}^{-1}$ integrated over the 50–300 keV band. (The integrated count rate over this band is used by BATSE to trigger bursts.) We folded each of their 54 best-fit models through the WFC response matrix and computed the ratio Φ_{WFC} of the WFC on-axis count rate to the 50–300 keV photon number flux. This may seem an odd ratio to take, but the WFC detectability is determined by the count rate, whereas the GRB flux distribution seen by BATSE is usually reported after correction for detector response, i.e. as a photon number flux. A histogram of these ratios, and of the more commonly used $F(2-10 \text{ keV})/F(50-300 \text{ keV})$, is shown in Fig. 2. The median flux ratio agrees with the Ginga estimates of 2–6% (Yoshida et al. 1989). But the large spread is crucial because it implies that a substantial fraction of GRB will be brighter than previous authors have estimated using a constant F_X/F_γ and will therefore be more easily detected.

A possible concern is the extent to which our sample is representative of the population. The selection criterion employed by Band et al. (1993) to obtain their subsample of the first BATSE catalogue for spectral fitting is essentially a brightness cut, and the authors consider the sample to be effectively a complete flux-limited one. This reduces the question of fair sampling to whether the spectral shape systematically changes with flux. There is one known effect of

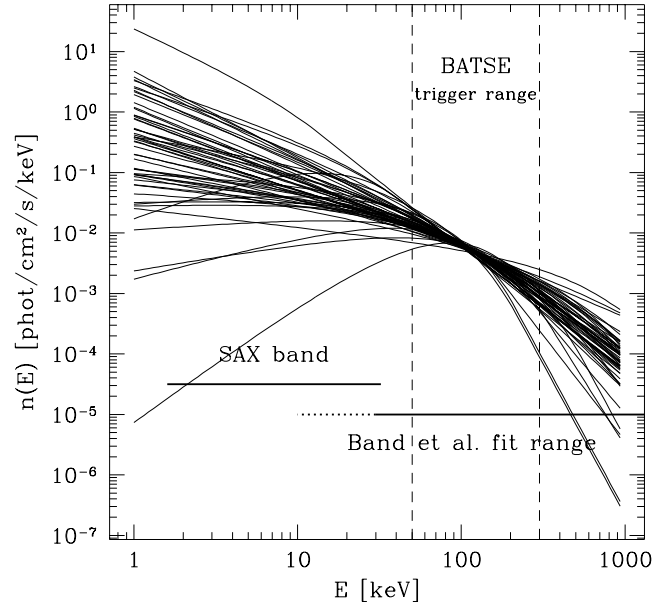


Figure 1. The best-fit model spectra for the GRB sample from Band et al. with their extrapolation into the WFC band. Note that the range over which the model fits were made significantly overlaps with the WFC band.

this kind, namely that faint bursts have break energies that are smaller by a factor 2 than bright ones (Malozzi et al. 1995). Since our spectral sample is from bright bursts, we may calculate the effect on the values of Φ_{WFC} by decreasing the value of the break flux by a factor 2 for the whole sample. Each value of Φ_{WFC} changes differently because the change depends on the spectral slopes, but the resulting distribution of Φ_{WFC} is shifted to higher values by a factor 2, i.e. faint bursts are relatively brighter in X rays.

Moreover, if there is a correlation between spectral shape and luminosity, and this is translated into a weak dependence of spectral shape on flux via the selection bias on flux, we probably should not even want to correct it because we will only see the most luminous bursts from M31 with SAX, so a sample of spectra that favours luminous bursts is a better one to use. Similarly, since the sample is gamma-ray selected, any bias in the spectral sample will be towards GRB that are gamma-ray bright, so the true population is likely to have on average greater X-ray brightnesses if the sample is not fair.

In what follows we shall use the Φ_{WFC} distribution from the Band et al. sample to estimate the X-ray detectability of GRB. We note that all the known and potential biases discussed would increase the number of detectable bursts from M31 over the calculations presented below.

2.3 X-ray detectability given a gamma-ray flux

To decide whether a given GRB will be detected by the WFC, we assume that it is a standard candle in the BATSE band. It has already been shown (Hakkila et al. 1995) that the range of gamma-ray luminosities of GRB must be small for all corona models that are still viable. Ulmer and Wijers (1995) also showed that for most luminosity functions, the luminosity distribution of detected GRB is narrow even if

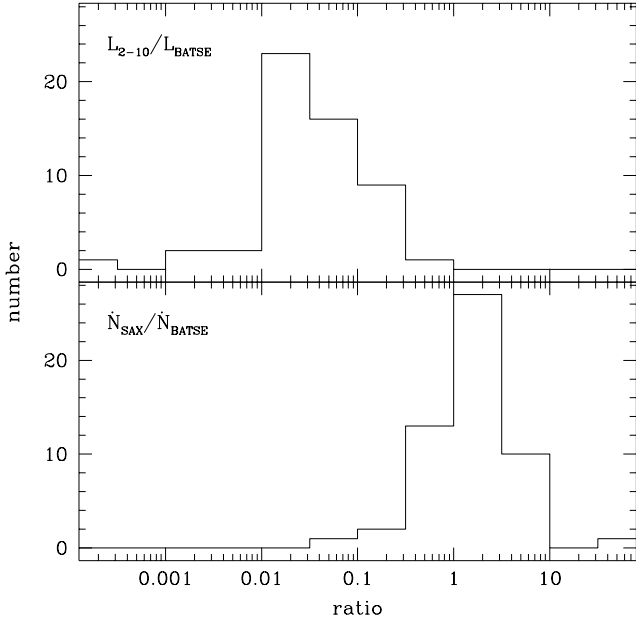


Figure 2. The distribution of classical X-ray flux (2–10 keV) to BATSE (50–300 keV) flux ratio (top) and the WFC (1.6–32 keV) to BATSE photon number flux ratio, which is more relevant for burst detection. The large difference is partly due to the energy per photon being much less in X rays, and partly due to the fact that the WFC band is much wider than the classical X-ray band.

the intrinsic luminosity function of the population is not. If the luminosity function is wide it increases the spread in X-ray luminosities at constant mean and therefore helps X-ray detection, unless there is a strong correlation between luminosity and spectral slope, so the standard-candle assumption will yield the lowest estimate of the number of X-ray detectable GRB.

The procedure to decide whether a model GRB will be detected by the WFC is then as follows. First, the 50–300 keV peak flux P_γ is given by the model. Then the WFC on-axis count rate is computed by multiplying with Φ_{WFC} . The model also specifies the location of the burst, from which we calculate the position (x, y) of its image in the detector plane (to be precise, the intersection of the line connecting the burst location and the centre of the mask with the detector plane). The count rate due to a burst at (x, y) is less than that due to one on axis by a factor $R(x, y)$, which accounts for the fact that it only illuminates a fraction of the detector and for the usual factor $\cos \theta$ to account for the fact that the detector plane is not perpendicular to the direction to the burst:

$$R(x, y) = \left(1 - \frac{|x|}{256}\right)\left(1 - \frac{|y|}{256}\right)\cos \theta. \quad (1)$$

(x and y are measured in mm from an origin at the detector centre, and the x and y axes are parallel to the edges of the square mask.) Given an integration time T and background count rate b , we get the total number of source counts $S = fP_\gamma\Phi_{\text{WFC}}RT$ and background counts $B = bT$. The factor f is required because P_γ is the peak flux, which will generally not be sustained for the full time T . In terms of the

instantaneous number flux $p_\gamma(t)$ from the burst (assumed 0 outside the interval $(0, T)$) we can formally define f as

$$f \equiv \frac{\int_0^T p_\gamma(t) dt}{P_\gamma T}, \quad (2)$$

Obviously, for a fixed value of T we will find a different f for each burst and f will usually be smaller for shorter bursts. We assume the background noise is Poissonian and large enough to be approximated by a normal distribution, so we can express the requirement that the burst be more than σ standard deviations above the background as a constraint on P_γ :

$$P_\gamma \geq P_\gamma^{\text{min}} \equiv \frac{\sigma\sqrt{b}}{f\Phi_{\text{WFC}}R(x, y)\sqrt{T}} \quad (3)$$

So we have now phrased the X-ray detectability as a constraint on the gamma-ray flux, which is convenient because most of the modelling of GRB populations is done in terms of the latter quantity. To account for the fact that Φ_{WFC} has a distribution of values rather than a fixed value, we treat a burst at a given (x, y) with a given P_γ as being detectable with probability

$$P_{\text{det}} = \frac{1}{54} \sum_{i=1}^{54} S(P_\gamma - P_{\gamma,i}^{\text{min}}), \quad (4)$$

where $S(x)$ is the Heaviside step function and we have defined $P_{\gamma,i}^{\text{min}}$ as the minimum detectable flux for the i th sample member. In other words, we just add up the fraction of model spectral shapes in the Band set for which its X-ray flux is above threshold. Since we do Monte Carlo simulations to find the rate of GRB detection (Sect. 3) we can then simply add up the P_{det} values in each sky and flux bin to get the detected rates.

In principle, the signal-to-noise of an off-centre source will be higher once it has been located, because the background need only be taken over the part of the detector that is illuminated by the source. However, we will not be aware of such sources until they are first noted in the full data stream so this does not change the detection rate.

For the preliminary investigation in this paper, we shall use $T = 20$ s and $f = 0.5$. This means we concentrate on the long part of the bimodal duration distribution of the bursts, which contains about 80% of the ones detected by BATSE. More advanced search techniques are clearly possible. For example, one can use a number of trial values of T or even trial sky positions for the bursts to enhance the sensitivity of the search. At the same time, this would increase the number of attempts at detection and therefore require a higher signal-to-noise threshold to avoid spurious signals. It is not meaningful in our view to explore these possibilities here because the optimal strategy will depend on details of the data set we will obtain. There will be real signals from other sources, such as X-ray bursts and flare stars, that may well constitute a higher contaminating rate than the expected foreground of Galactic GRB. A good fraction of those should be discernible from GRB on spectral or temporal grounds, but near the threshold complete subtraction may not be possible. Also, there could be instrumental effects that very occasionally give a spurious signal, and the importance thereof and consequences for the search and analysis strategy are hard to predict.

In Fig. 3 we show the detection probability for bursts at the centre of the detector field of view as a function of P_γ . The thick dashed curve is for BATSE, and the thick solid one is for the WFC using the nominal Band spectral set. Comparison of the two shows that above $0.3 \text{ phot cm}^{-2} \text{ s}^{-1}$ BATSE is more sensitive, but the curve for the WFC extends to well below the absolute limit for BATSE. This advantage vanishes if we look at bursts far away from the detector centre: 10° away along the detector diagonal the curve shifts up in flux by a factor 2.4, and 20° away that factor has grown to 12. So the effective field of view over which the WFC can probe fainter bursts than BATSE has a radius of about 10° .

There is one more spectral effect, however, that could dramatically increase the detected rate by the WFC: in a recent paper, Preece et al. (1996) find that many GRB have an excess flux above the Band et al. fits at energies between 5 and 10 keV. Inspecting their figure 5, it appears that about half of all GRB have an excess that is a factor 10 at 5 keV and decreases to near zero above 10 keV. To investigate the possible effect of this excess, we model it as a multiplicative factor C_{Preece} that is constant below 5 keV and decreases smoothly from 10 to 1 between 5 and 12 keV. To be precise, we multiplied the spectrum by

$$\begin{aligned} C_{\text{Preece}}(E) &= 10 & E < 5 \\ &= 1 + 4.5(1 + \cos \frac{\pi(E-5)}{7}) & 5 < E < 12 \\ &= 1 & 12 < E \end{aligned}$$

(with E in keV.) Adding this excess to each of the 54 spectra and recalculating the detection probabilities, we find that the entire sensitivity curve shifts down in flux by a factor of 7 (thin dashed curve in Fig. 3). Since only about half the bursts may have this excess, a more realistic case would be an even mixture of bursts with and without excess (thin solid curve). We stress that the fraction, f_{ex} , of bursts with excesses and the form of the excess are quite uncertain, so we explore the range $0.1 < f_{\text{ex}} < 0.9$ here. But since we will have spectra of all detected bursts in the eventual observations we can consistently account for it in the data, since even if no excess of GRB from M31 is found, a population of bursts with X-ray excesses would also greatly increase the foreground rate of GRB from our own Galaxy. Therefore we are in no danger of eventually overestimating the constraints on halo models from WFC data.

3 CORONA MODELS

For standard-candle gamma-ray bursts, the rate density of observable bursts as a function of distance from the centre of the corona follows directly from the observed $N(> P)$. It is usually approximated as

$$\rho(R) = \frac{\rho_0}{1 + (R/R_c)^\alpha} \quad (6)$$

and has three parameters, the central rate density ρ_0 , the core radius R_c , and the exponent α . Since the best values of α are small enough that the integrated density does not converge at large R , we have to add as a fourth parameter a cutoff radius of the corona, R_o , beyond which $\rho = 0$. An additional model parameter is the standard-candle gamma-ray photon emission rate \dot{N}_γ . It turns out that we only need

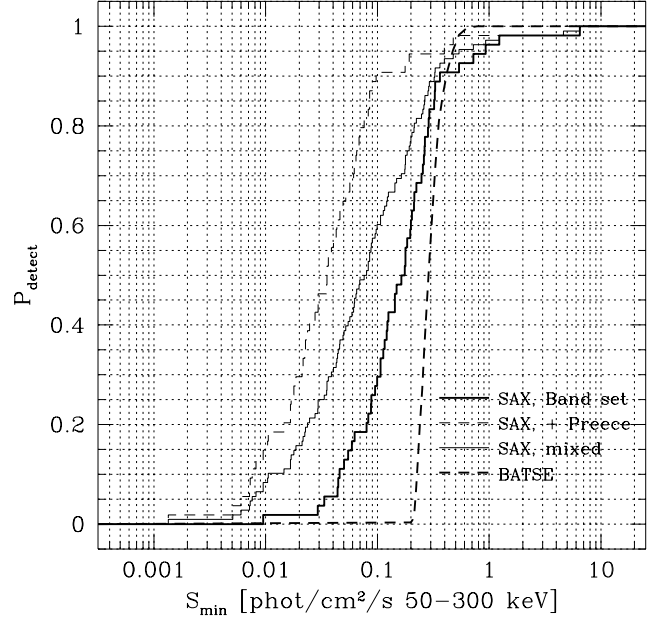


Figure 3. The detection probability of GRB at the centre of the WFC field of view compared with the BATSE trigger efficiency (thick dashed curve). The thick solid curve is for the Band et al. models; the thin dashed curve is with each burst given an X-ray excess suggested by the data from Preece et al. (see text). The thin solid curve is for a mixed population of 50% bursts with an X-ray excess and 50% without. The integration time for the WFC curves is 20 s, the background rate 130 cts s^{-1} , and the detection threshold is set at 5σ .

two of these, R_c and R_o , because the others follow from them if we use known observational constraints. Moreover, the results depend only weakly on R_o . We briefly indicate how a complete model is defined once the two radii are given: First, we note that the break in the counts slope from -1.5 to a smaller value occurs at $P_{\text{break}} = 20 \text{ phot cm}^{-2} \text{ s}^{-1}$. Since a burst with this flux is at distance R_c , this fixes the standard-candle value as $\dot{N}_\gamma = 4\pi R_c^2 P_{\text{break}}$. Next we use the fact that BATSE observes 300 bursts per year per 4π steradians above $P_{\text{comp}} = 1 \text{ phot cm}^{-2} \text{ s}^{-1}$. Because this flux is 20 times less than the break flux, it corresponds to a distance $R_c\sqrt{20}$, and we fix ρ_0 by requiring the integrated rate up to that distance to be 300/yr. α follows from the fact that $N(> P_\gamma) \propto P_\gamma^{-0.7}$ at the faint end of the BATSE distribution. Because the asymptotic counts slope at low fluxes for Eq. (6) is $(3-\alpha)/2$, this implies $\alpha = 1.6$. This completes the model for given R_c and R_o .

The reasonable range of R_c and R_o to explore is also limited by data. First, for $R_c \lesssim 30 - 40 \text{ kpc}$ BATSE would have detected an anisotropy due to our offset from the Galactic centre (Briggs et al. 1996b), and for $R_c \gtrsim 70 \text{ kpc}$ it would have seen M31. A minimum value for the outer radius follows from the fact that BATSE sees no sign of a truncation down to its 50% completeness limit of $0.28 \text{ phot cm}^{-2} \text{ s}^{-1}$. The distance to bursts of this flux is $8.5R_c$, i.e. at least 250 kpc, so we conclude that $R_o \gtrsim 250 \text{ kpc}$. Due to the low sensitivity of our results to R_o we fix it at half the distance to M31 in our calculations, noting that this is by no means required by all models. (For neutron-star ejection models with beaming, we use $R_o = 2 \text{ Mpc}$; see below.)

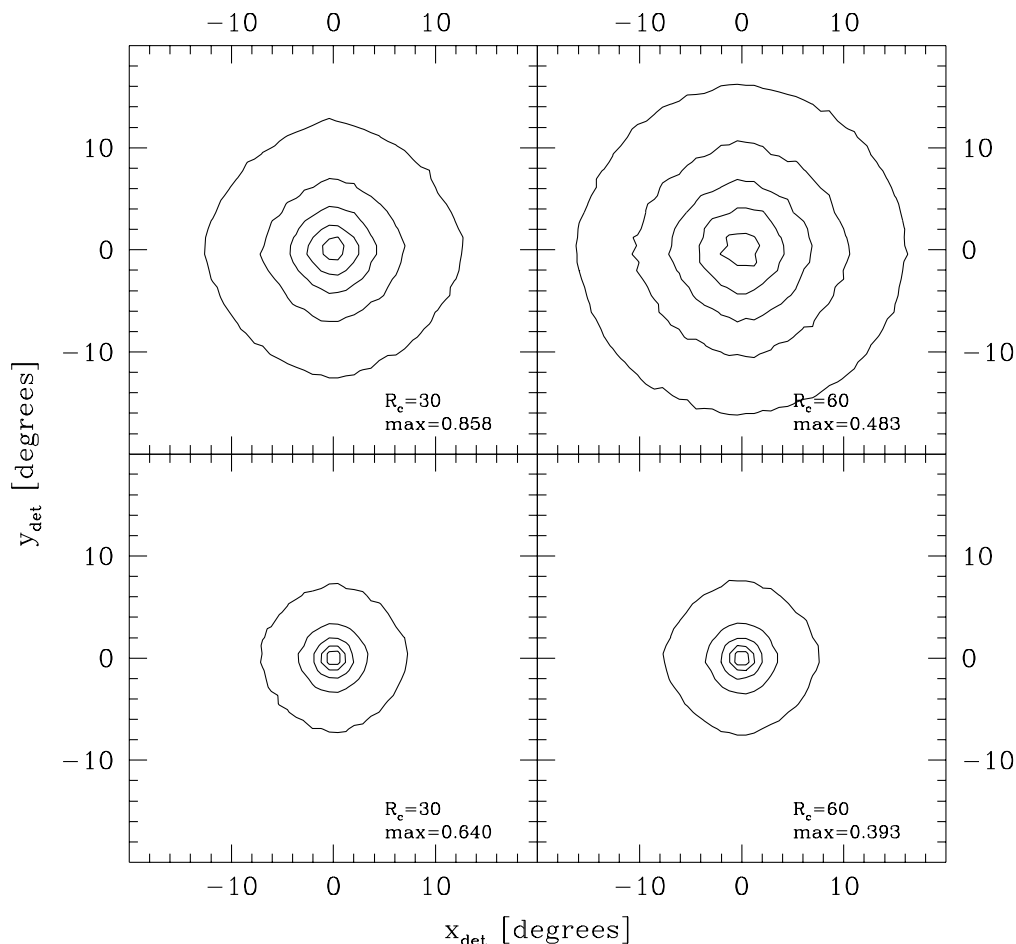


Figure 4. Four images of the rate of detectable bursts from M31. Contours at 10, 30, 50, 70, and 90% of the peak rate, which is indicated as ‘max’ in each panel (in units of $\text{deg}^{-2} \text{yr}^{-1}$). The x and y are offsets from the detector centre in degrees. All maps are made assuming 50% of GRB have an X-ray excess.

As stated, all standard-candle galactic-corona models have to satisfy this model for the effective rate density. Since non-standard-candle models have greater difficulty satisfying the BATSE constraints and also lead to easier detection of M31 we shall not consider them here. However, the net rate density is obtained in very different ways by different models, and this has some effect on detecting M31. It does not matter whether a static halo is used or one in which the bursters fly out of the Galaxy at high velocity, because all models of the latter type contain a provision of gradual or delayed turn-on of the bursting mechanism to ensure that the net rate density becomes the same again. However, some models (e.g. Duncan et al. 1993) invoke beaming of emission from fast neutron stars along their velocity direction to avoid anisotropy. The opening angle of the beams required in such models is of order the distance R_{GC} from us to the Galactic centre divided by R_c . This does matter, because it means that only bursters in M31 that move roughly towards or away from us will be seen. While this reduces the number of visible bursters, it also limits region of the sky where they are seen to a circle of angular radius about $R_c \sin \theta / D$ around the centre of M31, where θ is the opening angle of the beaming cone and D is the distance to M31. Since $\theta \simeq R_{GC} / R_c$ the angular radius is R_{GC} / D , independent of core radius. This area is quite small (typically a few square degrees) and therefore the background in it is very small, which may compensate for the lower expected rate to still give a detectable excess.

In our practical implementation, we used a Monte Carlo algorithm to create maps of the detectable rate of GRB per square degree per year from M31 and the Galactic foreground given a WFC pointing direction. The algorithm picks a burst in the Galaxy or M31 from the integrated density distribution between $R = 0$ and $R = R_o$ and random angular coordinates. Then we compute P_γ and the position on the sky, and from that the detection probability for the WFC. This probability is then added to the total in the appropriate sky location and/or flux bin and the procedure is repeated until the rate maps have sufficiently low Monte Carlo errors. In the case of beamed models, we also check whether the burst is shining in our direction before counting it as detectable. For this we make the approximation that GRB are ejected from a galaxy at such high velocities that they move at constant velocity in straight lines. We also assume they are all born at the centre of the galaxy and that their emitted flux is constant for all directions close enough to the direction of motion, and zero outside some critical angle. This simplification allows us to check the detectability of the burst using only the angle between our line of sight to the burst and the direction from the burst to the centre of M31. (This approximation is quite good, because the neutron star formation rate drops exponentially from the centre with a small scale length of only about 4 kpc, leading to an extra ‘smearing’ of the maps with an angular width of only $\theta_{\text{smear}} \sim 0.3^\circ$.) The opening angles (axis to edge) of the beaming cones we used for $R_c = 30, 40, 50, 60,$ and

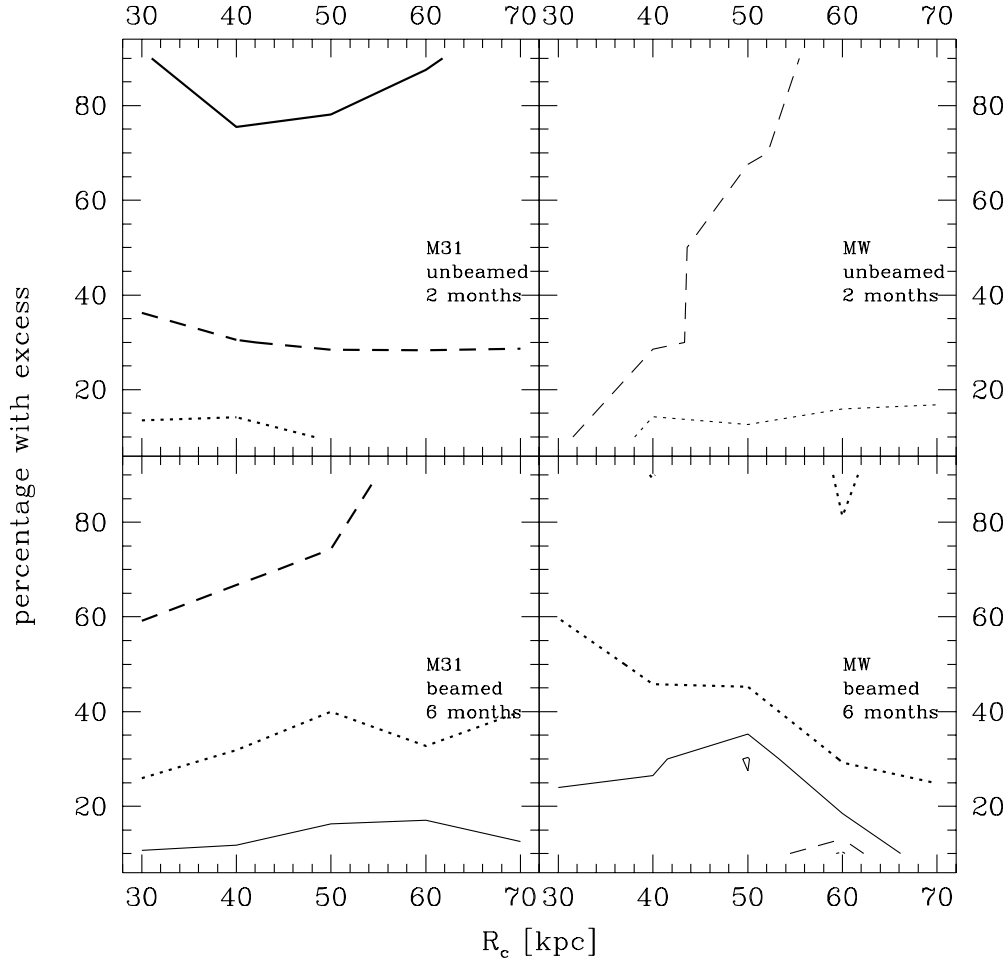


Figure 5. Contours of the expected number of bursts in a 2-month observation of unbeamed GRB (left) and a 6-month one of beamed GRB. The horizontal axis gives R_c , the vertical one the percentage of GRB with an X-ray excess. The contour values are 1 (thin-dotted), 2 (thin-dashed), 4 (thin-solid), 8 (thick-dotted), 16 (thick-dashed), and 32 (thick-solid). Left is the number from M31, right that from the Galactic foreground.

70 kpc are 20, 15, 12, 10, and 8 degrees, respectively, to keep $R_c\theta$ constant. Also, for these models we used outer radii of 2 Mpc for the halos. (They should be unlimited, but beyond that virtually no objects will be detectable.)

4 RESULTS

There are three main variables on which the detectability of an excess of GRB to M31 depends most: the core radius, the fraction of bursts, f_{ex} , with an X-ray excess, and beaming. To illustrate the dependence on R_c and beaming, we show in Fig. 4 maps of the detectable rate of GRB as a function of position on the sky (in number per square degree per year). The top panels are for unbeamed bursts, the bottom ones for beamed bursts. The influence of R_c is reflected by the differences between the left (30 kpc) and right (60 kpc) panels. As noted above, the image becomes much smaller for beamed bursts and the size is independent of R_c , whereas for unbeamed bursts the increase of the image size with R_c is clear. Also note the increased peak rate (labelled ‘max’ in each panel) for smaller core radii. This is because the central density scales as R_c^{-3} , and we do see a fair fraction of the bursts at the centre of M31. For comparison, the detectable rate from our own Milky Way is about 0.03/deg²/yr without beaming to 0.1/deg²/yr with beaming (the latter is greater due to the larger assumed outer radius for beamed models).

Because beaming so much reduces the area of sky over

which GRB can be seen, the total rate in the field of view will be much less for beamed bursts. This is very apparent in Fig. 5, in which we show the expected number of bursts as a function of parameters. The top panels show the expected numbers in a 2-month WFC camera observation with M31 in the centre of the field of view for unbeamed bursts. Notice how the number from M31 always dominates strongly. In the beamed models (bottom panels), however, the numbers from both are comparable and a much longer observation is needed to detect an excess towards M31.

Now we must create a practical test of whether seeing a certain number of GRB towards M31 constitutes evidence for or against a halo of GRB around it. Since the foreground bursts are more spread out on the sky than those of M31, this entails finding the optimum area of the detector to use as the region within which we look for bursts. A good choice of boundary turns out to be a contour on which the summed rate of M31 and Milky Way bursts is a fixed fraction of the summed peak rate. For a given set of halo model parameters, we then fix an observing time and a boundary. This completely specifies the expected number of bursts, E_{MW} , if there is no halo around M31, and the expected total number if there is, $E_{\text{MW}+\text{M31}}$. The actual numbers we would get in an observation, N_{MW} or $N_{\text{MW}+\text{M31}}$, have a Poisson distribution around the expected values. Let us choose a threshold value N_{th} , which defines the boundary between the accepting the null hypothesis H_0 ‘there is no halo with these pa-

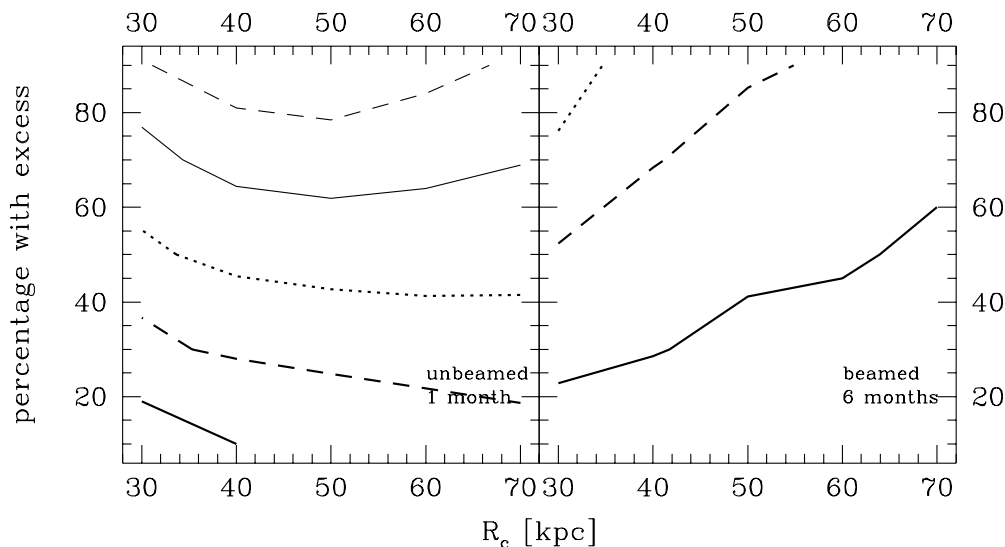


Figure 6. Contours of the probability of making the wrong decision based on a 1-month observation of unbeamed GRB (top) and a 6-month one of beamed GRB. The horizontal axis gives R_c , the vertical one the percentage of GRB with an X-ray excess, f_{ex} . The contour values range from 0.001 (thin-dashed) to 0.1 (thick-solid) in steps of $\sqrt{10}$.

rameters' and accepting the alternative H_1 'there is a halo with these parameters'. Obviously we can make two kinds of wrong decision: reject a halo when there is one, which happens with probability $P(N < N_{\text{th}} | E_{\text{MW}+\text{M31}}) \equiv P_1$, and accept one if there is none, which happens with probability $P(N \geq N_{\text{th}} | E_{\text{MW}}) \equiv P_2$. The best test will have small values of P_1 and P_2 ; Since we have no preference for either type of error above the other, we shall define N_{th} as the value for which $P_{\text{err}} = \max(P_1, P_2)$ is as small as possible. (The two can never be made equal because N_{th} can only assume integer values.) For a given halo model and observing time we can then further optimise the test by varying the boundary of the detector region inside which we accept bursts to get the lowest overall P_{err} . In practice the optimal contour boundary lies at a rate of 5–10% of the peak rate (but the minimum is shallow).

In Fig. 6 we show contours of optimised P_{err} values, again as a function of R_c and f_{ex} . We can see that for the nominal value $f_{\text{ex}} = 0.5$ we get a quite decisive test with $P_{\text{err}} < 0.01$ for all core radii if bursts are not beamed. The reason that the results do not depend as much on core radius as one might have thought is that sampling distance is not the major issue: the X-ray brightest bursts can be seen out to a few Mpc, well beyond M31. An increase in core radius will decrease the luminosity of bursts, but it will also increase the central density of the halo and concentrate the bursts more near the detector centre. The net effect is not large.

If GRB are beamed, P_{err} falls in the range 0.03–0.1 even for a 6-month observation, and the case is rather less convincing. Should the bursts be strongly beamed, our results point to a very cheap (in space dollars) and useful satellite mission that can settle the issue: a camera similar to the WFC, but with half the field of view and therefore only one quarter of the background. It should be pointed to M31 for 3–6 months and then in some other direction for a similar period of time and would either detect a corona of beamed sources or rule it out. Since many known X-ray sources in M31 would be easily detected in a small fraction of the required observing time by the same instrument, there would be considerable benefit to such a mission for the study of

variability and population analysis of bright X-ray binaries in M31.

5 DISCUSSION AND CONCLUSION

Previous work on constraining coronal models of GRB has many similarities with our own calculations. Liang (1991) found that ROSAT might detect some GRB in X rays assuming a now abandoned disc model for the distribution of GRB. Li, Fenimore, & Liang (1996) used a similar method to our own both for beamed and unbeamed models. Their calculations differ from ours mostly in that they use neither the spread in X-ray luminosity nor the X-ray excesses. Their hypothetical instrument had $S_{\text{min}} = 0.1 \text{ phot cm}^{-2} \text{ s}^{-1}$. As we can see from Fig. 3, 30–90% of the bursts that the WFC can see on-axis are below this limit, so it is no surprise that we find more optimistic prospects for detecting GRB in M31.

Harrison and Thorsett (1996) considered a variety of real instruments, calculating the detectable rate in much the same way as we did (including the spectral variability using the same set of spectra from Band et al. 1993). They conclude that only a novel instrument sensitive to photons in the 10–200 keV range and with a field of view of 18° would be capable of detecting M31 in one year. While they did not include the possibility of X-ray excesses, they would without doubt have realised the potential of the SAX WFC if they had included them in their work.

In summary, we have shown that the hitherto neglected spread in X-ray to gamma-ray luminosity ratios of gamma-ray bursts substantially increases the prospects for deciding the gamma-ray burst distance scale. The case is further improved greatly by the recent discovery that a substantial fraction of gamma-ray bursts have X-ray excesses (Preece et al. 1996). A one-month observation of M31 with an existing instrument, the SAX WFC, will be decisive for establishing whether or not the Andromeda Nebula harbours a population of bursters, unless bursters only emit radiation in fairly narrow cones along their direction of motion. In that case, a dedicated, cheap mission similar to the SAX WFC should resolve the issue in about one year of observing time. Observing proposals to do the experiment in WFC sec-

ondary (i.e. unguaranteed) time have been accepted, so the gamma-ray burst distance scale may not remain uncertain much longer.

ACKNOWLEDGEMENTS

MR thanks Steve Bell and the RGO summer school programme for the opportunity to work in Cambridge, and the IoA for hospitality. RAMJW thanks Arvind Parmar for pointing out the existence of the SAX WFCs to him and Martin Rees for very interesting discussions. This work was supported in part by grants BST 501/96 and 2 P304 016 07/94 (MR) and by PPARC (RAMJW).

REFERENCES

- Band, D., Matteson, J., Ford, L., Schaefer, B., Palmer, D., Teegarden, B., Cline, T., Briggs, M., Paciesas, W., Pendleton, G., Fishman, G., Kouveliotou, C., Meegan, C., Wilson, R., & Lestrade, P. 1993, *ApJ* 413, 281
- Briggs, M. S., Paciesas, W. S., Pendleton, G. N., Meegan, C. A., Fishman, G. J., Horack, J. M., Brock, M. N., Kouveliotou, C., Hartmann, D. H., & Hakkila, J. 1996b, *ApJ* 451, 40
- Briggs, M. S., Paciesas, W. S., Pendleton, G. N., Meegan, C. A., Fishman, G. J., Horack, J. M., Kouveliotou, C., Hartmann, D. H., & Hakkila, J. 1996a, in *Third Huntsville Symposium on Gamma-Ray Bursts*, eds. , C. Kouveliotou, M. S. Briggs, & G. J. Fishman (New York:AIP), p. in press
- Duncan, R. C., Li, H., & Thompson, C. 1993, in *Compton Gamma-Ray Observatory*, eds. , M. Friedlander, N. Gehrels, & D. J. Macomb, Vol. 280 of *AIP Conference Proceedings*, American Institute of Physics (New York:AIP), pp 1074–1079
- Fenimore, E. E., Epstein, R. I., Ho, C., Klebesadel, R. W., Lacey, C., Laros, J. G., Meier, M., Strohmayer, T., Pendleton, G., Fishman, G., Kouveliotou, C., & Meegan, C. 1993, *Nature* 366, 40
- Fishman, G. J. & Meegan, C. A. 1995, *ARA&A* 35, 415
- Hakkila, J., Meegan, C. A., Pendleton, G. N., m. Horack, J., Briggs, M. S., Paciesas, W. S., & gordon Emslie, A. 1995, *ApJ* 454, 134
- Hamilton, T. T., Gotthelf, E. V., & Helfand, D. J. 1996, *ApJ* 466, 795
- Harrison, F. A. & Thorsett, S. E. 1996, *ApJ* 460, L99
- Laros, J. G., Evans, W. D., Fenimore, E. E., Klebesadel, R. W., Shulman, S., & Fritz, G. 1984, *ApJ* 286, 681
- Li, H., Fenimore, E. E., & Liang, E. P. 1996, *ApJ* 461, L73
- Liang, E. P. 1991, *ApJ* 380, L55
- Malozzi, R. S., Paciesas, W. S., Pendleton, G. N., Briggs, M. S., Preece, R. D., Meegan, C. A., & Fishman, G. J. 1995, *ApJ* 454, 597
- Preece, R. D., Briggs, M. S., Pendleton, G. N., Paciesas, W. S., Matteson, J. L., Band, D. L., Skelton, R. T., & Meegan, C. A. 1996, *ApJ* 473, December 20
- Ulmer, A. & Wijers, R. A. M. J. 1995, *ApJ* 439, 303
- Yoshida, A., Murakami, T., Itoh, M., Nishimura, J., Tsuchiya, T., Fenimore, E. E., Klebesadel, R. W., & Evans, W. D. 1989, *PASJ* 41, 509